

## Four-Element Low-Band MIMO Antenna for Mobile Phones with Small Clearance

Harri Varheenmaa\*, Rasmus Luomaniemi, Anu Lehtovuori,  
Pasi Ylä-Oijala, and Ville Viikari

**Abstract**—This letter presents a four-element Multiple-Input Multiple-Output (MIMO) phone antenna with a metallic rim and 2-mm ground clearance that operates in the low-frequency band. Characteristic mode analysis is used to design the metallic rim so that the structure supports four resonating modes that can be excited separately to obtain MIMO operation in the desired frequency range below 1 GHz. Four exciter elements with matching circuits are designed so that the coupling between the ports is moderate. The prototype is manufactured, and measurement results are shown to corroborate the increased capacity compared to traditional two-element MIMO solutions.

### 1. INTRODUCTION

There is a continuous need for increased data transfer capacity, and therefore new frequency ranges are adopted for the use of cellular networks together with higher order Multiple-Input Multiple-Output (MIMO) [1]. In sparsely populated areas, lower frequencies are used for their better coverage, but the need for fast data transfer still exists. Thus, having antennas with high-order MIMO operation at lower frequencies is favorable. However, in the highly restricted antenna volume of current metal rim mobile devices, typically only three resonant modes exist at frequencies below 1 GHz [2].

Only a few four-element MIMO designs have been presented [3, 4]. The proposed designs have a large ground-plane clearance (even 11 mm), making them unusable in current devices, where the gap between the metal rim and the main body is only a few millimeters. In this challenging design environment, there are limited possibilities to make modifications to create new resonating modes, which are required to enable higher-order MIMO operation. Typically, fourth-order MIMO antenna has been implemented only at higher frequencies [5–8], and clearances are large even then. On the other hand, at 3.5 GHz, even eighth-order MIMO antenna has been proposed [9–11] with small clearances. Generally, the higher-order MIMO antennas reduce the probability that the user’s hand covers all antennas at the same time. This gives reason to increase the number of elements.

In this letter, we design a four-element MIMO antenna for the low-frequency band. With the aid of characteristic mode analysis (CMA), we modify the metal rim to support four resonating modes at frequencies below 1 GHz. By studying the resonance frequencies of the modes and their current distributions, we find four modes with sufficiently divergent currents and design a four-element feeding arrangement that provides a reasonable bandwidth. The measurement results for the prototype demonstrate that designing a capable four-element MIMO antenna is possible also with only a 2-mm clearance. The achieved ergodic capacity confirms increased data-transfer capability compared to the theoretical maximum of a two-element MIMO antenna.

---

*Received 14 May 2021, Accepted 11 June 2021, Scheduled 6 July 2021*

\* Corresponding author: Harri Varheenmaa (harri.varheenmaa@aalto.fi).

The authors are with the Department of Electronics and Nanoengineering, Aalto University, Espoo, P. O. Box 15500, Aalto 00076, Finland.

## 2. CMA ANALYSIS FOR ANTENNA DESIGN

Characteristic mode analysis is widely used in antenna design. Since CMA is independent of excitation, the electromagnetic properties of an antenna structure can be studied before implementing exciter elements [12]. Correspondingly, the positions of exciter elements can be determined based on resulting eigencurrent distributions [2].

The lack of resonating modes at lower frequencies complicates the design of MIMO antennas comprising more than two elements. To get a four-element MIMO antenna to operate as efficiently as possible, the antenna structure should support at least four resonating modes. A widely used approach to increase the number of resonating modes at low frequencies is to use a metallic rim around the antenna ground plane [2]. With an unbroken metal rim, only three modes resonate around 1 GHz [2]. In addition to the low number of modes, the bandwidth is inadequate for the desired band below 1 GHz in the unbroken-rim design.

In the case of an unbroken metal rim, the rim modes are full- and half-wavelength periodic at lower frequencies [2]. By splitting the rim, we can create new modes and also affect their resonance frequencies and current distributions. In this study, the current distributions of the modes of the broken rim are modified so that four-element MIMO antenna can be implemented. The idea of dividing the rim into smaller sections is to introduce a new fourth (rim) mode and change the eigencurrent distributions so that the current maxima of different modes do not overlap, and thus each mode can be excited selectively with the smallest possible coupling.

The number of modes and their bandwidth is studied by splitting the rim into three (case A) or four (case B) sections, as illustrated in Fig. 1. Naturally, the sections should be long enough to create modes that resonate in the desired frequency range. The fourth cut is used to get more freedom to design and modify the current distributions to facilitate separate excitation of modes. The final positions of the rim cuts are determined by analyzing how the cuts affect eigencurrent distributions, the resonance frequency, and frequency behavior of the modal significance.

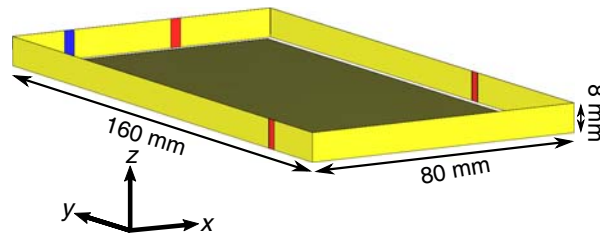


**Figure 1.** Dimensions of the device. The colour strips show the location of the rim cuts on the sides. Case A includes only red ones and case B includes both red and blue ones.

Using the CMA for Perfect Electric Conductor (PEC) structures [12], the locations of the cuts of the rim are found so that four resonating modes exist in the desired frequency band 824–960 MHz. Fig. 2 shows the modal significance of the modes when the rim is divided into three (case A) and four (case B) sections. The resonance frequencies of the modes can be tuned by changing the distance between the rim cuts. Four resonance modes at the target frequency range can be achieved with only three rim cuts if the rim is divided into three equal-length sections, each 159 mm which is about  $\lambda/2$  at around 0.9 GHz. The dashed lines in Fig. 2 show that the bandwidths of modes 2 and 3 are very narrow, whereas modes 1 and 4 have adequate bandwidths. By adding a fourth cut to the rim, the bandwidth of the narrowband modes can be widened. The position of the fourth rim cut, found by utilizing CMA, is shown in blue in Fig. 1. The additional cut does not have any significant effect on modes 1 and 4. However, the fourth rim cut shifts the resonances of all four modes a little higher in frequency, but this can be compensated with matching circuits.

Figure 3 shows the eigencurrent distributions of the modes at their resonance frequencies when the rim is cut into three sections. The rim modes 2–4 have the eigencurrent maxima at the same places, and thus efficient excitation of every single mode separately is difficult.

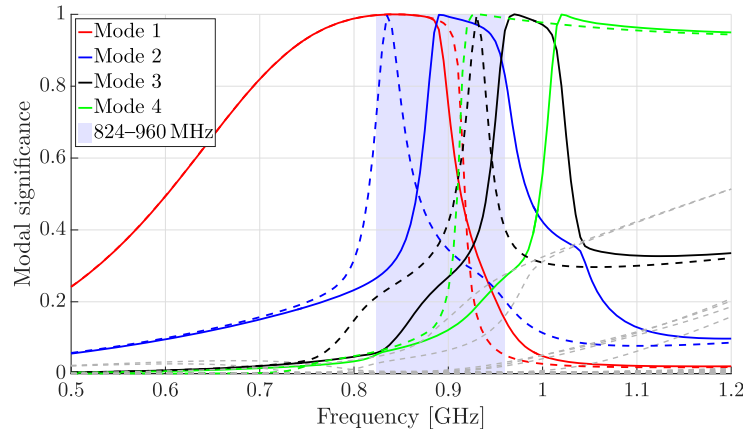


**Figure 2.** Modal significances of the modes. The results in case A are plotted with a dashed line and in case B with a solid line. The higher-order modes of both cases are plotted with grey dashed lines.

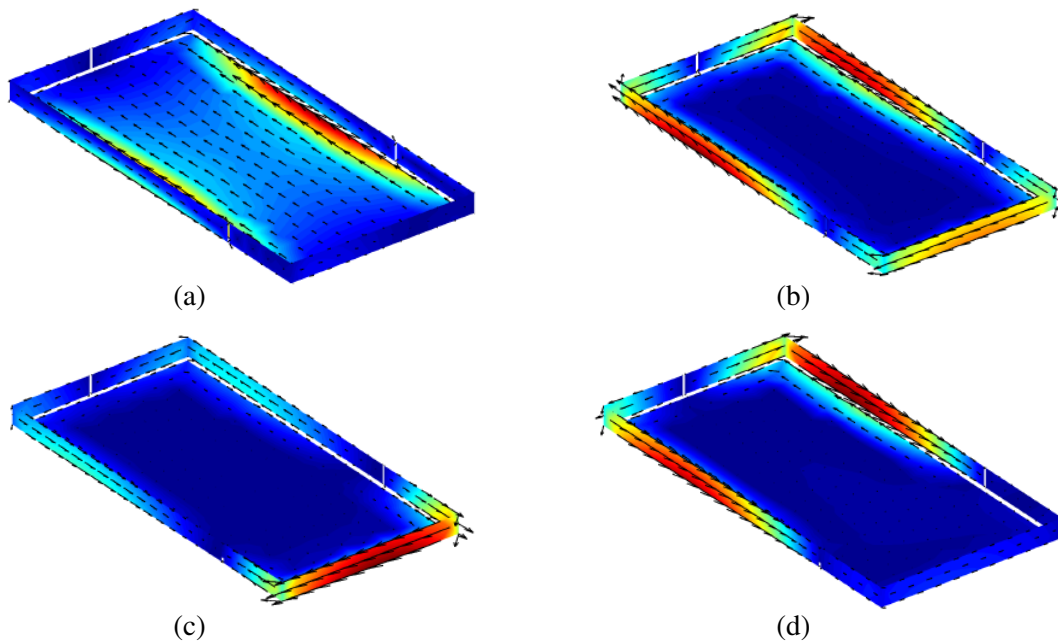


**Figure 3.** Eigencurrents of the modes at their resonance frequencies when the rim is divided into three equal-length sections (case A). (a) Mode 1 at 850 MHz, (b) Mode 2 at 835 MHz, (c) Mode 3 at 930 MHz, (d) Mode 4 at 930 MHz.

Figure 4 illustrates the eigencurrent distributions when the fourth cut is added to the rim. The fourth rim cut breaks similarity in the eigencurrent distributions, which facilitates selective excitation of the modes with only moderate coupling between them. This gives a promising starting point for the actual antenna design.

### 3. ANTENNA DESIGN

The eigencurrent distributions of the modes assists finding the optimum placement for the exciter elements. The location of capacitive exciter favors the current minimum whereas the location of inductive exciter prefers the current maximum [2]. In addition to the exciter element location, the used exciter element type affects bandwidth and how well modes are excited. Previous studies have

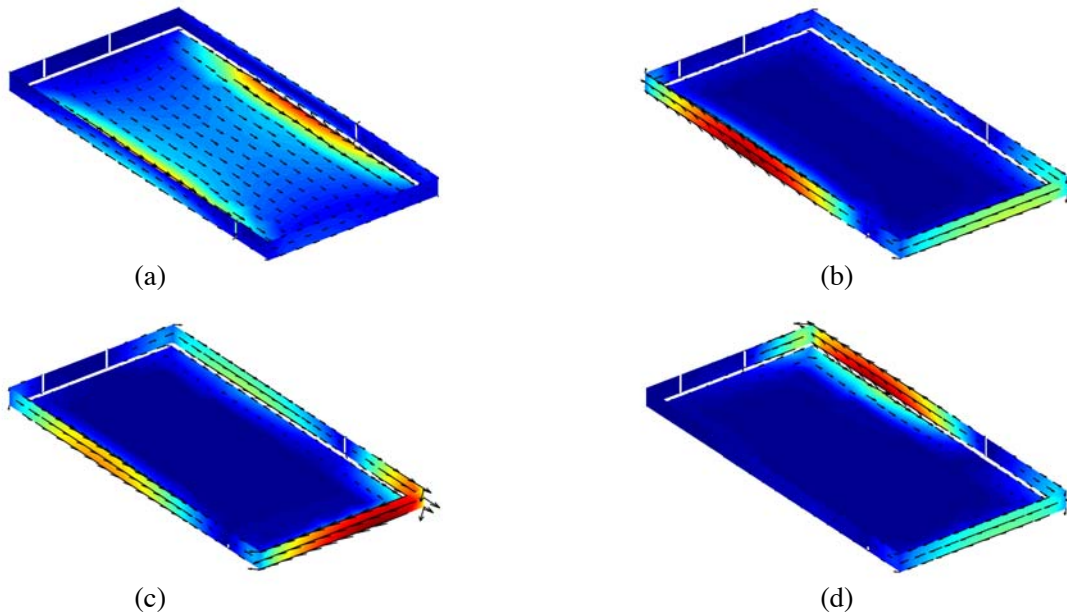


**Figure 4.** Eigencurrents of the modes at their resonance frequencies when the rim is divided into four sections (case B). (a) Mode 1 at 845 MHz, (b) Mode 2 at 890 MHz, (c) Mode 3 at 970 MHz, (d) Mode 4 at 1020 MHz.

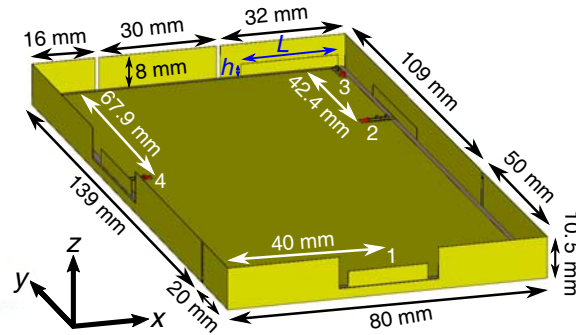


**Figure 5.** Dimensions of the antenna. Locations of the ports 1–4 are marked in white, and  $L$  and  $h$  are the length and height, respectively, of the feeding elements. Part of the rim is removed for better visualization.

used, e.g., T- and L-shaped exciter elements [2] and strips that connect the rim and the ground plane together [13]. Since the ground clearance of the proposed device is small (2 mm), both T- and L-shaped exciter elements are bent parallel to the rim (see Fig. 5). In this phase, it is important to also consider the effect of matching circuits [14]. An ideal three-component matching circuit has been designed using Optenni Lab [15] for each exciter element. The matching circuits are found so that the total efficiency is maximized.

The results indicate that all rim modes can be excited efficiently with T-shaped feeding elements placed at the current maximum (elements 1, 2, and 4 in Fig. 5). However, in addition to the clear current maximum, each rim mode has a rather strong current concentration on another edge of the rim, as can be seen in Fig. 4. Due to the partly overlapping strong currents, the modes cannot be excited purely independently, and therefore, there appears coupling between the corresponding ports. In addition, the ground-plane mode can be excited with an L-shaped element placed at the current minimum (element 3 in Fig. 5). Thus, the ground-plane mode 1 can be excited so that the coupling with rim modes 2 and 4 is decreased.

#### 4. PROTOTYPE AND RESULTS

The proposed antenna structure is designed next with realistic materials and components. The exciter elements and metal rim are made of laser-cut 0.1-mm thin copper. The copper ground plane and component pads are on a low-loss 1.524-mm thick Rogers RO4350B substrate ( $\epsilon_r = 3.66$  and  $\tan(\delta) = 0.0037$ ). A supporting structure milled out of a low-loss Preperm RS260 plastic ( $\epsilon_r = 2.58$  and  $\tan(\delta) = 0.0009$  at 2.4 GHz) is used to place the copper rim and exciter elements. The supporting plastic structure is milled so that the printed circuit board (PCB) is placed inside of it. There is about a 1-mm layer of the support plastic under the PCB. On each side of the support structure, there are also milled support walls to which the rim and exciter elements are glued to. The matching circuits are realized with size 0402 Murata GJM15 capacitors and the same size Coilcraft 0402DC inductors.

The dimensions ( $d$ ,  $h$ , and  $L$ ) of the exciter elements are re-optimized after the plastic support structure is added to the simulation model. Fig. 5 illustrates the final design, and Table 1 shows the final dimensions of exciter elements. The three-component matching circuits with realistic components in Fig. 6 are also optimized with Optenni Lab.

**Table 1.** Dimensions of the final exciter elements.  $d$  is the distance between the rim and the exciter element.

Exciter	1	2	3	4
$h$ [mm]	4	3	3	4
$L$ [mm]	20	35	25	25
$d$ [mm]	0.47	0.62	0.62	0.5

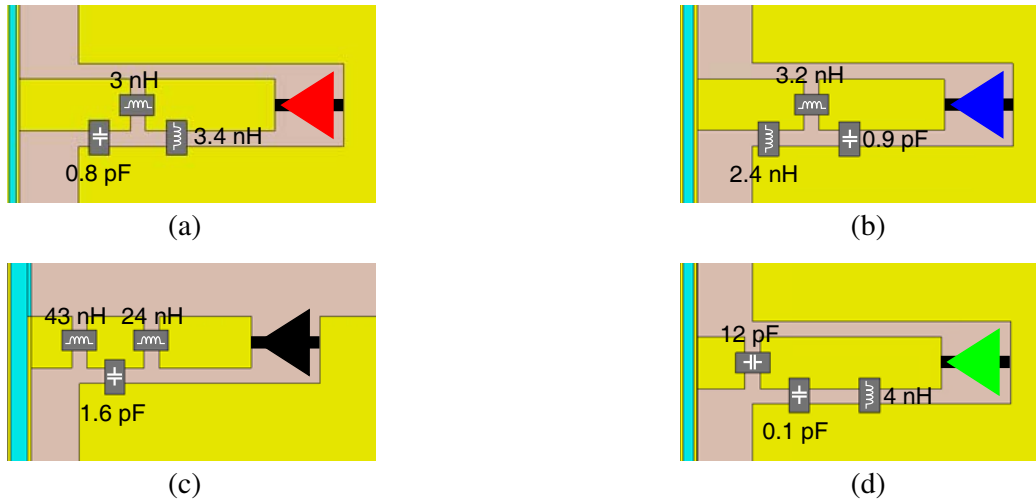


**Figure 6.** Matching circuits of the final design. (a) Port 1, (b) Port 2, (c) Port 3, (d) Port 4.

A prototype of the antenna was manufactured, and the fabricated antenna design is shown in Fig. 7. Radiation pattern measurements are done with the Microwave Vision Group StarLab antenna measurement system, and  $S$ -parameters are measured with a two-port Vector Network Analyzer (VNA). The far-field patterns are measured one port at a time, and the unconnected ports are terminated with 50- $\Omega$  load.

The simulated and measured  $S$ -parameters are shown in Figs. 8 and 9. These figures show that the measured  $S$ -parameters are over-tuned, but all ports are matched in the same frequency range, 900–1010 MHz. The coupling is lower in the measured antenna than in the simulated one. The frequency shift between the simulations and measurements is likely caused by manufacturing defects in the support plastic.

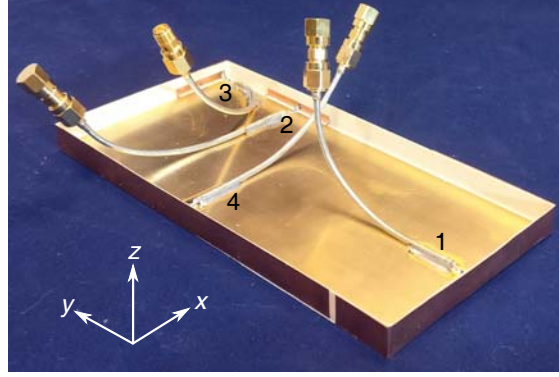


**Figure 7.** Manufactured prototype.

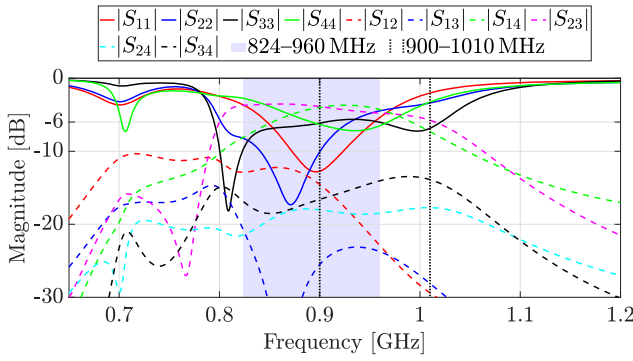


**Figure 8.** Simulated  $S$ -parameters.

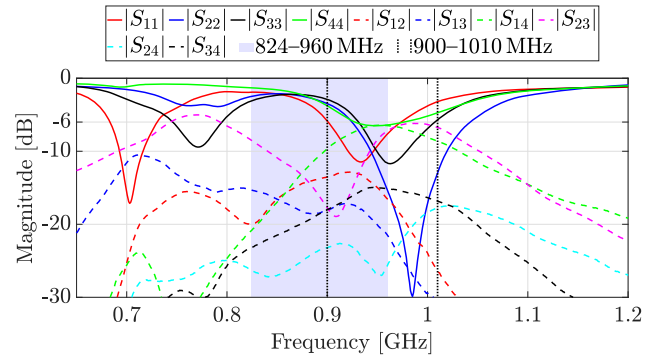


**Figure 9.** Measured  $S$ -parameters.

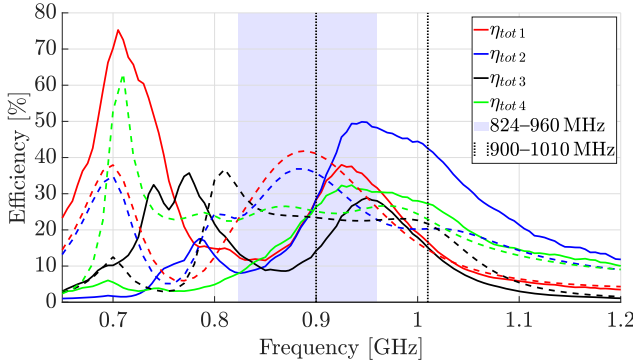


**Figure 10.** Simulated and measured total efficiency. The measured values are plotted with a solid line and the simulated with a dashed line.

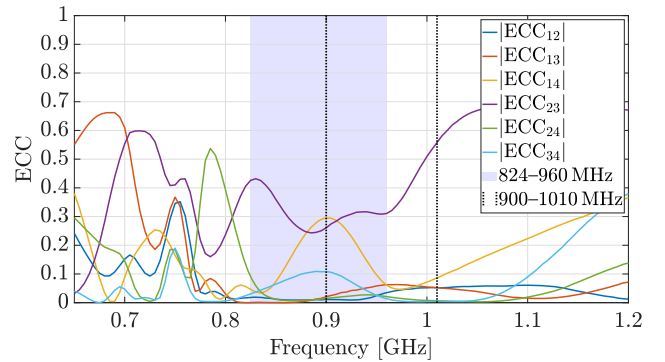


**Figure 11.** ECC, calculated from the measured far-field pattern.

Figure 10 shows the simulated and measured total efficiencies. According to simulations, the total efficiency is about 22–42% in the target frequency range (824–960 MHz). Correspondingly, due to the frequency shift, the operation frequency moves to 900–1010 MHz. In this frequency range, the measured total efficiency is 15–50%.

Figure 11 shows the enveloped correlation coefficient (ECC), which is calculated from measured far-field patterns [16]. The commonly used  $< 0.5$  limit is achieved in almost the whole frequency band (at 1010 MHz,  $ECC_{23}$  is 0.55). The calculated ergodic capacity [17] is shown in Fig. 12. The ergodic capacity, both in the simulations and for the prototype, is calculated using an Signal-to-Noise Ratio

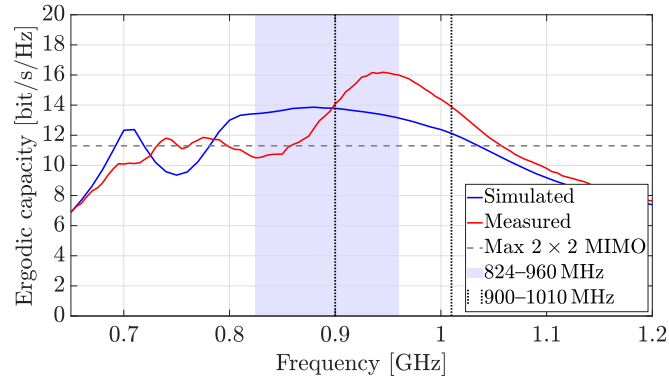


**Figure 12.** Ergodic capacity. The theoretical maximum ergodic capacity of a two-element MIMO is plotted with the grey dashed line.

(SNR) of 20 dB and a Rayleigh fading channel realizations of  $10^4$ , both of which are typical values. In Fig. 12, the theoretical maximum capacity of the  $2 \times 2$  MIMO antenna is illustrated with a grey dashed line. The proposed four-port MIMO antenna performs better than commonly-used two-element MIMOs in the entire operation band.

A comparison of previously studied low-band MIMO mobile antennas is presented in Table 2. The achieved total efficiency (15–50%) is in line with previous studies. The attained ergodic capacity (14–16.2 bit/s/Hz) is greater than the theoretical one for two-element MIMOs (11.3 bit/s/Hz) in which the majority of low-band MIMO mobile antennas can at most exhibit. In addition, the achieved ergodic capacity is at the same level as that of the previously studied four-element MIMO antenna with much larger ground clearance [3].

**Table 2.** Comparison of previously studied low-band MIMO mobile antennas.

Ref.	MIMO order	Clear. min/ max [mm]	Freq. band [MHz]	$\eta_{tot}$ %	Cap. [bit/s/Hz]
<b>Sim.</b>			824–960	22–42	13.1–13.9
<b>Meas.</b>	4	2	900–1010	15–50	14–16.2
[18]	2	3/5	824–960	15–59	7.3–9.8
[2]	2	3/8	742–1000	15–78	—
[19]	2	2/8	824–960	36–48	8.5–9.6
[20]	2	2/10	824–960	31–38	—
[3]	4	1/10	824–960	30–46	16–16.9
[4]	4	11	824–960	25–42	—

## 5. CONCLUSION

CMA has been used to find four low-band modes for a small-ground-clearance mobile antenna structure. Bandwidth properties and different current distributions of the modes make designing a small-ground-clearance four-element MIMO mobile antenna possible. The antennas operate in the 900–1010 MHz band, and they exhibit good values in both efficiency and capacity, especially for such small ground clearance. The performance is competitive compared to previously published designs, and the achieved capacity is greater than the theoretical value of commonly used two-element low-band MIMO mobile antennas.

## ACKNOWLEDGMENT

The authors would like to thank Albert Salmi for his help in manufacturing and measuring the prototype.

## REFERENCES

1. Varzakas, P., "Average channel capacity for Rayleigh fading spread spectrum MIMO systems," *International Journal of Communication Systems*, Vol. 19, No. 10, 1081–1087, 2006. [Online]. Available: <https://onlinelibrary.wiley.com/doi/abs/10.1002/dac.784>.
2. Deng, C., Z. Feng, and S. V. Hum, "MIMO mobile handset antenna merging characteristic modes for increased bandwidth," *IEEE Transactions on Antennas and Propagation*, Vol. 64, No. 7, 2660–2667, Jul. 2016.
3. Wong, K.-L., Y.-C. Chen, and W.-Y. Li, "Four LTE low-band smartphone antennas and their MIMO performance with user's hand presence," *Microwave and Optical Technology Letters*, Vol. 58, No. 9, 2046–2052, 2016. [Online]. Available: <https://onlinelibrary.wiley.com/doi/abs/10.1002/mop.29969>.
4. Anguera, J., A. Andújar, R. M. Mateos, and S. Kahng, "A  $4 \times 4$  MIMO multiband antenna system with non-resonant elements for smartphone platforms," *2017 11th European Conference on Antennas and Propagation (EUCAP)*, 2705–2708, Mar. 2017.
5. Li, M., Y. Ban, Z. Xu, G. Wu, C. Sim, K. Kang, and Z. Yu, "Eight-port orthogonally dual-polarized antenna array for 5G smartphone applications," *IEEE Transactions on Antennas and Propagation*, Vol. 64, No. 9, 3820–3830, Sep. 2016.
6. Huang, D., Z. Du, and Y. Wang, "A quad-antenna system for 4G/5G/GPS metal frame mobile phones," *IEEE Antennas and Wireless Propagation Letters*, Vol. 18, No. 8, 1586–1590, Aug. 2019.
7. Barani, I. R. R. and K. Wong, "Integrated inverted-F and open-slot antennas in the metal-framed smartphone for  $2 \times 2$  LTE LB and  $4 \times 4$  LTE M/HB MIMO operations," *IEEE Transactions on Antennas and Propagation*, Vol. 66, No. 10, 5004–5012, Oct. 2018.
8. Wong, K.-L., C.-C. Wan, and L.-Y. Chen, "Self-decoupled compact metal-frame LTE MIMO antennas for the smartphone," *Microwave and Optical Technology Letters*, Vol. 60, No. 5, 1170–1179, 2018. [Online]. Available: <https://onlinelibrary.wiley.com/doi/abs/10.1002/mop.31129>.
9. Ren, A., Y. Liu, and C. Sim, "A compact building block with two shared-aperture antennas for eight-antenna MIMO array in metal-rimmed smartphone," *IEEE Transactions on Antennas and Propagation*, Vol. 67, No. 10, 6430–6438, Oct. 2019.
10. Sun, L., Y. Li, Z. Zhang, and H. Wang, "Self-decoupled mimo antenna pair with shared radiator for 5G smartphones," *IEEE Transactions on Antennas and Propagation*, Vol. 68, No. 5, 3423–3432, May 2020.
11. Chen, H., Y. Tsai, C. Sim, and C. Kuo, "Broadband eight-antenna array design for sub-6 GHz 5G NR bands metal-frame smartphone applications," *IEEE Antennas and Wireless Propagation Letters*, Vol. 19, No. 7, 1078–1082, Jul. 2020.
12. Harrington, R. and J. Mautz, "Theory of characteristic modes for conducting bodies," *IEEE Transactions on Antennas and Propagation*, Vol. 19, No. 5, 622–628, Sep. 1971.
13. Deng, C., Z. Xu, A. Ren, and S. V. Hum, "TCM-based bezel antenna design with small ground clearance for mobile terminals," *IEEE Transactions on Antennas and Propagation*, Vol. 67, No. 2, 745–754, Feb. 2019.
14. Lehtovuori, A., R. Valkonen, and J. Ilvonen, "Designing capacitive coupling element antennas with bandwidth estimators," *IEEE Antennas and Wireless Propagation Letters*, Vol. 13, 959–962, 2014.
15. Optenni Oy. Optenni Lab. Accessed: 26.03.2021. [Online]. Available: <https://www.optenni.com/>.
16. Thaysen, J. and K. B. Jakobsen, "Envelope correlation in (N, N) MIMO antenna array from scattering parameters," *Microwave and Optical Technology Letters*, Vol. 48, No. 5, 832–834, 2006. [Online]. Available: <https://onlinelibrary.wiley.com/doi/abs/10.1002/mop.21490>.
17. Tian, R., B. K. Lau, and Z. Ying, "Multiplexing efficiency of MIMO antennas," *IEEE Antennas and Wireless Propagation Letters*, Vol. 10, 183–186, 2011.

18. Luomaniemi, R., J. Hannula, R. Kormilainen, A. Lehtovuori, and V. Viikari, "Unbroken metal rim MIMO antenna utilizing antenna clusters," *IEEE Antennas and Wireless Propagation Letters*, Vol. 18, No. 6, 1071–1075, Jun. 2019.
19. Xu, Z., Y. Sun, Q. Zhou, Y. Ban, Y. Li, and S. S. Ang, "Reconfigurable MIMO antenna for integrated-metal-rimmed smartphone applications," *IEEE Access*, Vol. 5, 21 223–21 228, 2017.
20. Zhang, L., Y. Ban, C. Sim, J. Guo, and Z. Yu, "Parallel dual-loop antenna for WWAN/LTE metal-rimmed smartphone," *IEEE Transactions on Antennas and Propagation*, Vol. 66, No. 3, 1217–1226, Mar. 2018.